Spray Coating Experiments: Setups and Methodologies

The latest eBook from Advanced Optical Metrology. Download for free.

Spray Coating Experiments: Setups and Methodologies, is the third in our Thin Films eBook series. This publication provides an introduction to spray coating, three article digests from Wiley Online Library and the latest news about Evident's Image of the Year Award 2022.

Wiley in collaboration with Evident, are committed to bridging the gap between fundamental research and industrial applications in the field of optical metrology. We strive to do this by collecting and organizing existing information, making it more accessible and useful for researchers and practitioners alike.

EVIDENT
OLYMPUS

WILEY

NANO · MICRO small
www.small-journal.com

End-Group Engineering of Chlorine-Trialkylsiylthienyl Chain-Substituted Small-Molecule Donors for High-Efficiency Ternary Solar Cells

Jing Li, Chenyang Zhang, Xiuzun Zhong, Wanyuan Deng, Hanlin Hu, and Kai Wang**

Ternary architecture has been widely demonstrated as a facile and efficient strategy to boost the performance of organic solar cells (OSCs). However, the rational design of the third component with suitable core and end-group modification is still a challenge. Herein, two new small-molecule (SM) donors BT-CN and BT-ER, featuring the identical conjugated backbone with distinct end group, have been designed, synthesized, and introduced into the PM6:Y6 binary system as the second donor. Both molecules exhibit complementary absorption and good miscibility with PM6, contributing to the nanofibrous phases and strong face-on molecular packing. Importantly, the incorporation of BT-CN/BT-ER has significantly facilitated charge collection and transportation with remarkable suppression of carrier recombination. As a result, ternary OSCs with 20 wt% BT-CN/BT-ER achieved a PCE of 16.8%/17.22% with synchronously increased open-circuit voltage (V_{OC}), short-circuit current density (J_{SC}) and fill factor (FF). Moreover, replacing Y6 with L8-BO further improves the PCE to 18.05%/18.11%, indicating the universality of both molecules as the third component. This work demonstrates not only two efficient SM donors with 4,8-bis(4-chloro-5-(tripropylsilyl)thiophen-2-yl) benzo[1,2-*b*:4,5-*b*′]dithiophene (BDTT-SiCl) as the core but also end group modification strategy to fine-tune the absorption spectrum, molecular packing, and energy levels of SM donors to construct high-performance ternary OSCs.

1. Introduction

Bulk-heterojunction (BHJ) organic solar cells (OSCs), as one of most promising photoelectric transform technology, ascribed to fabricate lightweight and flexible large-area device via solution processing, have a pivotal position in commercial-oriented applications in the future.[1–5] In the last three years, OSCs have got great strides forward that attributes to emerging non-fullerene small molecular (SM) acceptors of Y6 and its derivatives,[6–11] and power conversion efficiency (PCE) of the single-junction OSC device has achieved over 19%.[12–14] Despite the remarkable achievements, the development of binary OSCs is still limited by some intrinsic shortcomings, particularly the trade-off between the current density (J_{SC}) and V_{OC}.[2,15,16] For instance, the initially designed low-bandgap material Y6 can deliver a high J_{SC} for PM6:Y6 binary device, yet result in a relatively low V_{OC},[17–19] consequently hindering the further enhancement of device performance. In this regard, the fabrication of ternary OSCs by incorporation of a third component into the binary system offers a facile and effective approach to solve this issue.[20–24] Ternary OSCs can combine the advantages of tandem solar cells, which achieve enhanced photon harvesting, and retain the simple processing of single-junction devices. A suitable third component can not only broaden the absorption and thus contribute the J_{SC} value, but also facilitate the charge transfer and/or reduce carrier recombination to enhance J_{SC} and fill factor (FF).[25–29] The third component can play a critical role in energy alignment, which directly influence the V_{OC} of the final device. The appropriate third component can enhance the luminescence and suppress the energy loss, resulting in increased V_{OC}. Moreover, since the long-term stability of OSCs has been recognized the biggest challenge for future commercialization, the introduction of an appropriate third component has been proven to enhance the stability of the devices.[19,30,31] It is worth mentioning that most of the third components in ternary OSC are fullerenes and nonfullerene acceptors so far.[32,33] Recently, SM donors have attracted extensive research attention as the third compound due to their definite molecular structure, simple synthesize route, and easier purification.[34,35] Moreover, SM donors generally possess strong crystallinity, which might be more desirable to optimize the morphology of ternary blend film.[36–41] However, the development of SM donor as the guest material lags behind the acceptor counterpart because

J. Li, C. Zhang, X. Zhong, K. Wang
Institute of Flexible Electronics (IFE)
Northwestern Polytechnical University (NPU)
Xi'an 710072, P. R. China
E-mail: kaiwang@nwpu.edu.cn
C. Zhang, H. Hu
Hoffman Institute of Advanced Materials
Shenzhen Polytechnic
7098 Liuxian Boulevard, Shenzhen 518055, P. R. China
E-mail: hanlinhu@szpt.edu.cn
W. Deng
Institute of Polymer Optoelectronic Materials and Devices
State Key Laboratory of Luminescent Materials and Devices
South China University of Technology
Guangzhou 510641, P. R. China
The ORCID identification number(s) for the author(s) of this article can be found under https://doi.org/10.1002/smll.202205572.

DOI: 10.1002/smll.202205572

it is more challenging to simultaneously satisfy the request of energy levels and absorption.

In the last year, ternary OSCs with PM6:Y6 as the binary host and SM donor as the guest component have shown a rapid development, and the PCE of corresponding devices has exceeded 17%.[42,43] Tan et al. developed a SM donor of BTBR-2F adopting difluorobenzene-octylthiophene units as π bridge to form noncovalent conformational locking. Ternary device incorporating 20 wt.% of this molecule achieved a high PCE of 17.38%.[44] Zhao et al. synthesized an asymmetric SM donor, TTBT-R. The resulting ternary device with an appropriate amount of TTBT-R reached a high PCE of 18.07%.[45] Ge et al. utilized dithienosilole as π bridge to fine-tune the microstructure morphology, the ternary OSC based on PM6:G19:Y6 showed a PCE of 17.86%.[46] Many efforts have been put into the regulation of the middle core and π linker.[43,47–54] However, the detailed impact of end-groups of SM donor on the performance of ternary OSCs has received less attention. It is worth noting that end groups of the molecular backbone play a significant influence on the optoelectronic and aggregation properties of the material.

Cyanoacetate end group has been proven as a class of good moiety to construct efficient small molecule donors in binary OSCs, and the esterified rhodamine end group can finely adjust the crystallinity and improve the charge mobilities of the resulting molecule.[55] Whereas, the effect of these two end groups in ternary OSCs has not been studied. On the other hand, it was reported the introduction of trialkylsilyl and Cl atom onto the thienyl BDT core (BDTT-SiCl) can reduce HOMO (highest occupied molecular orbital) level, increase the absorption coefficient and hole mobility, as well as modulate the morphology.[56–58] Polymer and SM donors incorporating trialkylsilyl and Cl atom substituted BDTT core have achieved promising efficiency in binary devices.[59] Inspired by the achievement of the BDTT-SiCl core, herein, we developed two SM donors BT-CN and BT-ER, composed of BDTT-SiCl middle core, and π bridge of dioctyl-terthiophene linked via distinct end-group of cyanooctyl ester and esterified rhodanine, respectively. The end groups are proven to be able to fine-tune the electronics and crystalline properties of the SM donors. Both SM donors have been utilized to fabricate ternary OSCs and study the influence of end groups on the final performance of ternary OSCs. Both SM donors exhibit complementary absorption and good miscibility with PM6:Y6 blend. Besides, the energy levels of these two SM donors are parallel to that of PM6, and the morphology of the ternary device based on these two molecules shows improved crystallinity, more favorable face-on packing, and a well-mixed phase. Device characterization illustrates the introduction of the SM donors as the guest component has enhanced the charge transport and collection ability, meanwhile suppressing the carrier recombination process. As a result, ternary OSCs with 20 wt.% BT-CN/ BT-ER achieves a PCE of 16.8% /17.22% due to the simultaneously increased V_{OC}, $J_{SC,}$ and FF in contrast to the PM6:Y6 binary device. Moreover, when replacing Y6 with L8-BO, ternary device incorporating these two SM donors can both reach an exhilarating PCE of over 18%. Specifically, the ternary OSCs with 15 wt.% of BT-ER deliver the best PCE of 18.11% with a V_{OC} of 0.908 V, J_{SC} of 26.72 mA cm$^{-2,}$ and FF of 74.67%, indicating the universality of these two SM donors as the third component for highly efficient PM6 based ternary OSCs. These results demonstrate the SM analogs both perform comparably well in ternary OSCs, suggesting that BDTT-SiCl-substituted SMs are a quite promising class of SM donors for ternary OSCs.

2. Results and Discussion

2.1. Synthesis and Properties

The molecular structures of PM6, Y6, BT-CN, and BT-ER are shown in **Figure 1**a. Both SMs take trialkylsilyl and Cl substituted thienyl benzo[1,2-*b*:4,5-*b'*]dithiophene (BDTT-SiCl) as the middle core. It has been featured with π bridge of dioctyl-terthiophene combined with varied end group of cyanooctyl ester for BT-CN, and esterified rhodanine for BT-ER. The synthetic routes of BT-CN and BT-ER are shown in Scheme S1 in Supporting Information (SI). The target molecules of BT-CN and BT-ER were successfully obtained through the Stille coupling reaction with a yield of 64.8% and 67.4% for BT-CN and BT-ER respectively. Both of them exhibit good solubility and can be dissolved in common solvents such as chloroform, chlorobenzene, and so on., and both structures are characterized by ^{1}H NMR, ^{13}C NMR, and high-resolution mass spectroscopy (Figure S1-S6, Supporting Information). Thermogravimetric analysis (TGA) shows that BT-CN and BT-ER possess high thermal stability with a decomposition temperature (T_d, 5% weight loss) of 353 °C and 370 °C under nitrogen atmosphere, respectively (Figure S7, Supporting Information).

The UV–Vis absorption spectra of PM6, Y6, BT-CN, and BT-ER in both the solid films and chloroform solutions are shown in Figure 1b. In chloroform solution, the maximum absorption peak of BT-ER (500 nm) redshifts 14 nm than BT-CN (486 nm). Both BT-CN and BT-ER film exhibit strong absorption in the range of 400–650 nm. The maximum absorption peak is located at 555 nm and 567 nm for BT-CN and BT-ER, respectively, providing complementary absorption with PM6:Y6 blend film, which benefits to elevate J_{SC} of the ternary device. In contrast to the BT-CN, the slight redshift of BT-ER both in solid film and solution state indicates that the esterified rhodanine end-group in BT-ER has a stronger electron-withdrawing ability, resulting in a stronger intramolecular interaction. The optical bandgap (E_g^{opt}) was calculated to be 1.89 eV and 1.85 eV, respectively.

Density functional theory (DFT) calculations have been applied to evaluate the energy levels and conformations of the two SM donors (Figure S8–S9, Supporting Information). All the alkyl chains were simplified to the methyl group to reduce the complexity of calculation.[60] The HOMO/LUMO levels derived from the calculations are −5.39/−3.17 eV and −5.32/−3.18 eV for BT-CN and BT-ER, respectively. Cyclic voltammetry (CV) measurement (Figure S10, Supporting Information) is performed to evaluate HOMO energy levels by the formula of $E_{HOMO} = -E$ ($E_{onset,\ Ox}$ + 4.80−$E_{Fc/Fc+}$) (eV),[61] in which $E_{Fc/Fc+}$ is the redox potential of Fc/Fc$^+$ (0.55 eV versus Ag/AgCl). The HOMO levels of BT-CN and BT-ER are −5.42/−5.41 eV, respectively. The lowest unoccupied molecular orbital (LUMO) levels are calculated to be −3.53/−3.56 eV for BT-CN and BT-ER, respectively, according to formula $E_g^{opt} = E_{HOMO} - E_{LUMO}$. The estimated energy levels show the same trend as the results derived from DFT calculation. Figure 1c shows the energy level diagrams of PM6, Y6, BT-CN,

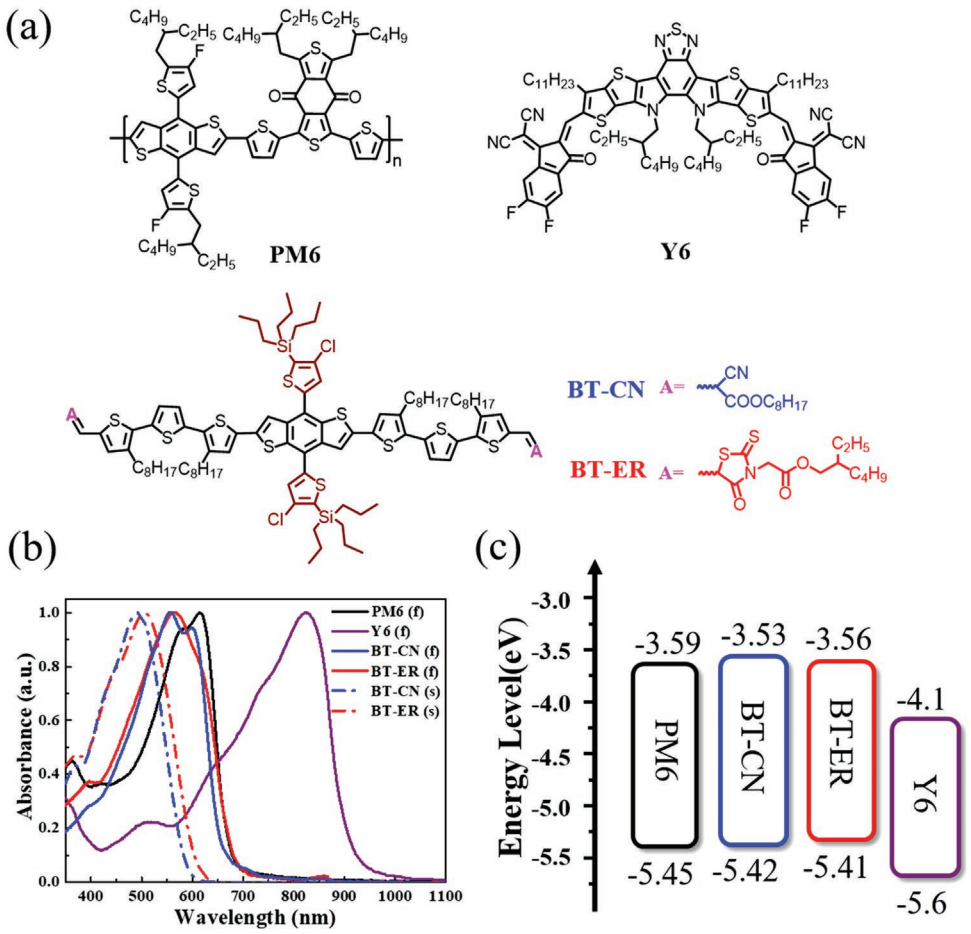

Figure 1. a) Chemical structures of PM6, Y6, BT-CN, and BT-ER. b) UV–vis absorption spectra of PM6, Y6, BT-CN, and BT-ER in solution and film state. c) Energy levels alignment of PM6, Y6, BT-CN, and BT-ER.

and BT-ER. The photoluminescence (PL) spectra of pristine PM6, BT-CN, BT-ER and their blend films of PM6:BT-CN, PM6:BT-ER were characterized to explore the electron transfer behavior between PM6 and the two SM donors (Figure S11, Supporting Information). The neat films of PM6, BT-CN, and BT-ER show a strong emission peak at 680, 695, and 732 nm when excited at 532 nm, respectively. Turning to the blend film of BT-ER/BT-CN with PM6 (1:5, w/w), both of PL emission spectrum shows an obvious fluorescence quenching compared with the pristine films, which implies that there would be an energy transfer between PM6 and BT-CN/BT-ER.[62]

2.2. Photovoltaic properties

To examine the effect of BT-CN and BT-ER as third component on device photovoltaic performance, ternary OSCs with inverted device architecture of ITO/ZnO/active layer/MoO_3/Ag were fabricated. All the devices were prepared by spin-coating chloroform solution fixing PM6:Y6 ratio of 1:1.2. Various ratios of BT-CN or BT-ER (10%, 15%, 20%, 30%, by weight ratio) were added into PM6:Y6 blend to systematically construct the ternary blend. The ternary OSCs were optimized by adjusting the D/A ratio and the annealing temperature (Table S1–S4, Supporting Information). The optimal devices' photovoltaic parameters were summarized in **Table 1**. The current density-voltage (J–V) curves of the binary and ternary OSCs were all measured under simulated AM1.5G sun illumination (100 mW cm^{-2}) in ambient conditions without encapsulation. The control PM6:Y6 binary device exhibits an average efficiency of 15.51% with V_{OC} of 0.826 V, J_{SC} of 26.21 mA cm^{-2} and FF of 71.63%, which is in parallel with the reported values.[17] With the addition of BT-CN or BT-ER, the photovoltaic performance of the OSCs has been improved. When blending with 20 wt.% BT-CN, the ternary device achieved a PCE of 16.8% with a V_{OC} of 0.838 V, J_{SC} of 27.38 mA cm^{-2}, and an FF of 73.23%. Similarly, addition of 20 wt.% BT-ER delivered a high PCE of 17.22% with a V_{OC} of 0.841 V, J_{SC} of 27.64 mA cm^{-2} and FF of 74.11%. This can be attributed to the enhanced absorption in the short wavelength and possibly optimized morphology of the active layer. The representative J–V curves and statistical distribution of PCE from 10 devices are depicted in **Figure 2**a,b. Further addition of BT-CN or BT-ER (30 wt.%) leads to reduced J_{SC} and FF, which might be due to a poor morphology of the active layers. For the BT-CN/BT-ER: Y6 binary system, it just exhibits a PCE of 8.33% and 6.55%, respectively (Table S5 and Figure S12a, Supporting Information). These photovoltaic results demonstrate that the introduction of these two SM donors as the

Table 1. Summary of photovoltaic performance of the optimized binary and ternary devices.

Active layer[a)]	V_{OC} (V)	J_{SC} (mA cm^{-2})	FF (%)	PCE (%)
PM6:Y6	0.826(0.822 ± 0.0072)	26.21(26.29 ± 0.59)	71.63(72.00 ± 0.54)	15.51(15.46 ± 0.32)
PM6:BT-CN:Y6	0.838(0.8360 ± 0078)	27.38(27.387 ± 0.15)	73.23(72.751 ± 0.61)	16.80(16.66 ± 0.1)
PM6:BT-ER:Y6	0.841(0.845 ± 0.0045)	27.64 (27.31 ± 0.18)	74.11 (73.90 ± 0.38)	17.22 (17.05 ± 0.08)
PM6:L8-BO	0.888(0.887 ± 0.0019)	26.14(26.18 ± 0.031)	75.60(75.59 ± 0.26)	17.55(17.55 ± 0.10)
PM6:BT-CN:L8-BO	0.908(0.909 ± 0.004)	26.76(26.71 ± 0.08)	74.27(74.11 ± 0.13)	18.05(17.99 ± 0.04)
PM6:BT-ER:L8-BO	0.908(0.908 ± 0.0019)	26.72(26.81 ± 0.07)	74.67(74.21 ± 0.26)	18.11(18.06 ± 0.03)

[a)]The average values within the parentheses were obtained with 10 devices.

third component in PM6:Y6 binary system could efficiently improve the device performance by simultaneously benefiting all the parameters. The ternary OSC based on BT-ER shows slightly higher performance than that of BT-CN-based device. The measured J_{SC} from *J–V* curves agrees well with the integrated J_{SC} extracted from external quantum efficiency (EQE) spectra within a 5% error. Figure 2c emphasizes the significant contributions in the short wavelength region in the EQE.

2.3. Charge Transportation, Recombination, and Energy Loss

Space charge limited current (SCLC) method was utilized to study the transportation property of the ternary device, which is summarized in Figure S13 and Table S6, Supporting Information. The hole/electron mobility of the PM6:Y6, PM6:BT-CN: Y6 and PM6:BT-ER:Y6 are $1.05 \times 10^{-4}/1.43 \times 10^{-4}$, $1.46 \times 10^{-4}/2.02 \times 10^{-4}$ and $2.61 \times 10^{-4}/3.45 \times 10^{-4}$ (cm^2 V^{-1}s^{-1}), respectively. The ternary device exhibits slightly elevated hole/electron mobility after introducing the third component, which might be attributed to the increased crystallization and improved out-of-plane orientation.[63] The exciton dissociation process of the binary and ternary devices was explored by the relationship between photocurrent density (J_{ph}) and effective voltage (V_{eff}). Generally, J_{ph} is defined as $J_{ph} = J_L - J_D$, where J_L is the light current densities and the J_D is dark current densities. V_{eff} is defined as $V_{eff} = V_0 - V$, where V represents the applied voltage and V_0 signifies the voltage when $J_{ph} = 0$. The ratio of J_{ph}/J_{sat} (J_{sat} is the density of the saturated photocurrent when V_{eff} exceeds 2.0 V) can be used to characterize the exciton dissociation probability $P(E, T)$.[21,64] As shown in Figure 2d, the $P(E, T)$ value is 90% for PM6:BT-ER:Y6 and 89% for PM6:BT-CN:Y6, respectively. Compared to 87% for PM6:Y6 binary system, the increased $P(E, T)$ values suggest a more efficient charge collection process for the ternary devices.

The dependence of J_{SC} and V_{OC} on light intensity of ternary devices was measured to explore the charge recombination. The correlation between J_{SC} and the light intensity (P_{light}) is described by the formula $J_{SC} \propto P_{light}^{\alpha}$, α is defined as the exponential

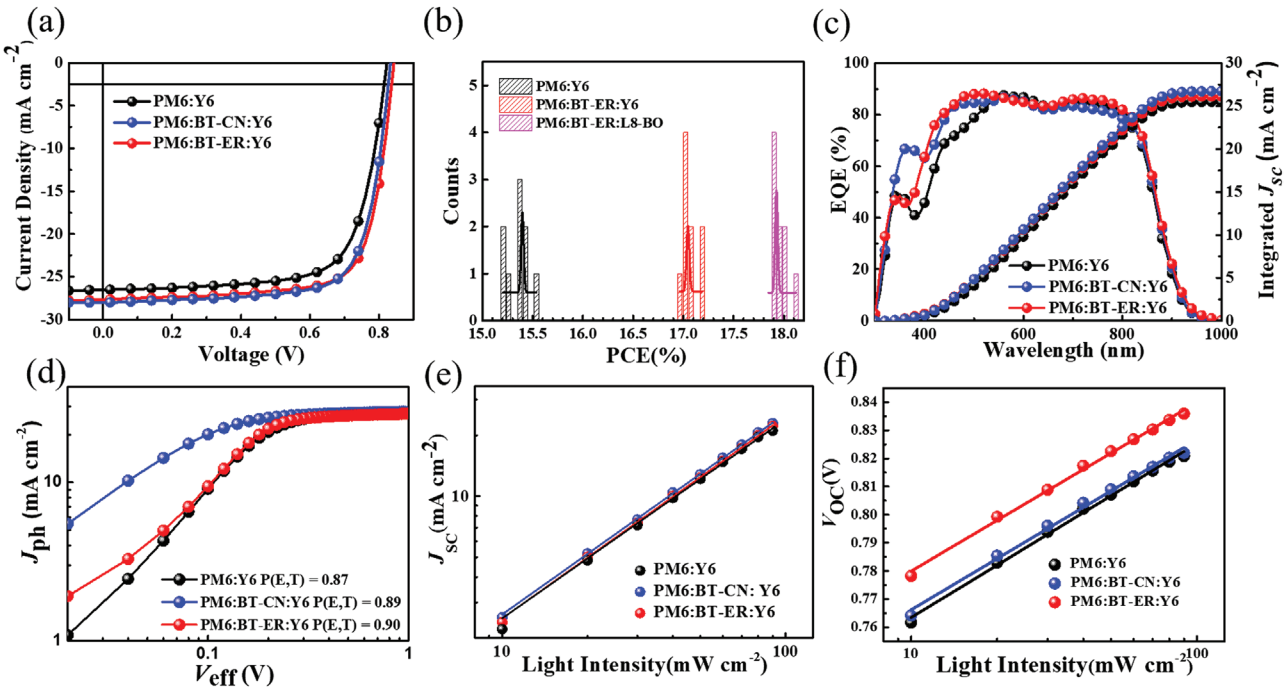

Figure 2. a) *J–V* curves for optimized OSCs. b) Statistical distribution of PCE binary and ternary devices based on BT-ER. c) EQE spectra and integrated current densities for optimized OSCs. d) J_{ph} –V_{eff} curves. e) J_{SC} and f) V_{OC} versus light intensity.

Table 2. Detailed energy losses of PM6:Y6 binary device, PM6:BT-CN:Y6 and PM6:BT-ER:Y6 ternary device.

Device	E_g^{PV} [eV]	V_{oc}^{Cal} [V]	qV_{oc}^{SQ} [eV]	qV_{oc}^{rad} [eV]	ΔE_1 [eV]	ΔE_2 [eV]	ΔE_3 [eV]	E_{loss} [eV]	EQE_{EL} ($\times 10^{-2}$%)
PM6:Y6	1.39	0.823	1.131	1.069	0.259	0.062	0.246	0.567	0.75
PM6:BT-CN:Y6	1.39	0.844	1.31	1.070	0.26	0.06	0.226	0.546	1.6
PM6:BT-ER:Y6	1.39	0.845	1.131	1.070	0.259	0.061	0.225	0.545	1.7

factor, which is used to describe the charge recombination.[53] The α value of PM6:BT-ER:Y6, PM6:BT-CN:Y6 are 0.997 and 0.991, respectively, higher than that of PM6:Y6 binary system (0.965), indicating the bimolecular recombination is further suppressed in ternary device than a binary device (Figure 2e). Figure 2f shows the relationship between V_{OC} and P_{light}, and it is defined as $V_{OC} \propto (nkT/e) \ln(P_{light})$.[65] K is the Boltzmann constant, T is the absolute temperature, and e is the elemental charge. The slope values for PM6:BT-CN:Y6, PM6:BT-ER:Y6 are 1.01KT/e and 1.00 KT/e. Both values are smaller than PM6:Y6 (1.07 KT/e), referring to a lower trap-assisted recombination in the ternary device.

To evaluate the end-group effect on the energy loss (E_{loss}), we performed Fourier-transform photocurrent spectroscopy external quantum efficiency (FTPS-EQE) and electroluminescent (EL) spectra in the optimized binary and ternary devices.[66,67] The details of each component of the E_{loss} are shown in **Table 2** and Figure S14, Supporting Information. The term $\Delta E_1 = E_g - qV_{oc}^{SQ}$ represents the inevitable radiative recombination owing to the absorption above the E_g. The next term ΔE_2 is radiative loss caused by absorption below the bandgap.[68,69] As shown in Table 2, it is apparent the incorporation of the SM donors has little impact on the radiant ΔE_1 and ΔE_2. The nonradiative recombination loss ΔE_3 was estimated via calculating the electroluminescent quantum efficiency (EQE_{EL}). The ternary devices show enhanced EQE_{EL}, corresponding a smaller ΔE_3 (0.225 eV for PM6:BT-ER:Y6 and 0.226 eV for PM6:BT-CN:Y6) compared to 0.246 eV of the binary device. This result indicates that the nonradiative recombination loss in the ternary devices was successfully suppressed. The calculated E_{loss} is 0.567, 0.546, and 0.545 eV for PM6:Y6, PM6:BT-CN:Y6, and PM6:BT-ER:Y6, respectively, consistent with the V_{OC} of the corresponding OSCs. The optimal BT-ER-based ternary device afforded slightly lower E_{loss}, therefore gave rise to a higher V_{OC}.

2.4. Morphology Analysis

Differential scanning calorimetry (DSC) was used to characterize the melting and miscibility behavior of BT-ER/BT-CN, PM6, and Y6 (**Figure 3**a-c). As shown in Figure 3a, BT-CN and BT-ER reveal apparent endothermic peaks at 215.41 °C and 183.34 °C in the heating process, respectively. PM6 doesn't show any melting or crystallization peak in the range of measured temperature. The PM6:BT-CN and PM6:BT-ER (5:1, w/w) mixtures do not show any peak of BT-ER/BT-CN, which suggests both molecules are well miscible with PM6 (Figure 3b).[70] Y6 possesses a melt peak at 296.91 °C. However, the melting peak of Y6 and BT-CN mixture (6:1, w/w) decreases to 291.61 °C. The peak at 211.39 °C should be ascribed to the melt of BT-CN, indicating partially miscible between Y6 and BT-CN. Likewise, the Y6 and BT-ER mixture (6:1, w/w) shows an indistinct broad peak at 287.44 °C and a weak peak at 180.86 °C, which could be the melting peak of BT-ER. Therefore, most of the molecules should be dispersed in PM6 domain with a minor part distributed in the Y6 domain in the ternary film. To further understand the miscibility of the two SM donors with PM6 and Y6, contact angle measurements of deionized water and ethylene glycol as the calibrated liquids (Figure 3d) has been conducted. The detailed data was displayed in Table S7, Supporting Information.

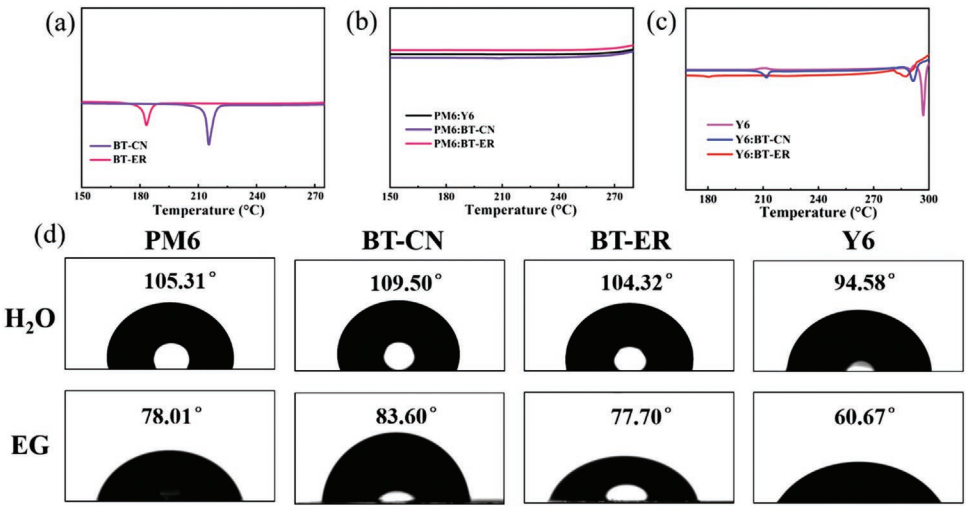

Figure 3. DSC curves of a) BT-CN and BT-ER. b) PM6, PM6:BT-CN and PM6:BT-ER. c) Y6, Y6:BT-CN, and Y6:BT-ER during the heating process. d) Contact angle images of water and ethylene glycol drops on PM6, BT-CN, BT-ER, and Y6 films.

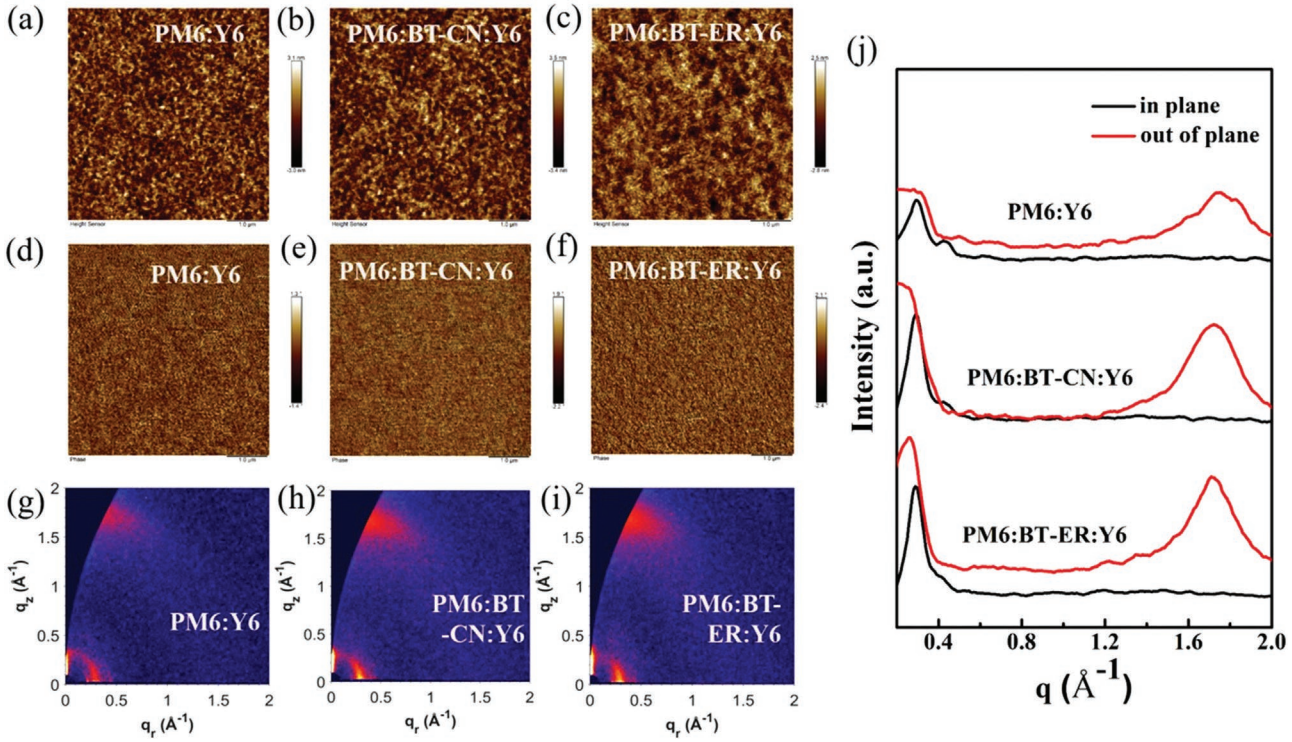

Figure 4. AFM height images a) PM6:Y6, b) PM6:BT-CN:Y6, c) PM6:BT-ER: Y6. AFM phase images d) PM6:Y6, e) PM6:BT-CN:Y6, f) PM6:BT-ER:Y6. GIWAXS images of blends g) PM6:Y6; h) PM6:BT-CN:Y6; i) PM6:BT-ER:Y6. j) GIWAXS intensity profiles along in-plane direction and out-of-plane direction.

The calculated surface energy (SFE) values for PM6, Y6, BT-ER, and BT-CN were 25.08, 37.03, 22.05, and 27.05 mJ m^{-2}, respectively. The Flory–Huggins interaction parameter (χ) based on the SFE of the above materials was calculated according to the formula $\chi = K(\sqrt{\gamma D} - \sqrt{\gamma A})^2$.[71] The calculated χ value of PM6:BT-CN and Y6:BT-CN are 0.098 K and 1.93 K, while the χ value of PM6:BT-ER and Y6:BT-ER is 0.037 K and 0.78 K, Both molecules present smaller χ values with PM6 than with Y6, proving both of them are more miscible in PM6, rather than in Y6 (Table S7, Supporting Information). In addition, the relatively smaller χ value of BT-ER with PM6 indicates that BT-ER might be more easily miscible with PM6 than BT-CN.

Atomic force microscopy (AFM) was performed to investigate the top surface morphology of the binary and optimized ternary blend films. **Figure 4**a-f shows AFM height images and phase images of the optimized binary and ternary blend films, and those of BT-CN:Y6 and BT-ER:Y6 blend films were shown in Figure S15, Supporting Information. The root-mean-square (RMS) roughness value is 0.867, 0.985, and 0.754 nm for PM6:Y6, PM6:BT-CN:Y6, and PM6:BT-ER:Y6 blend film, respectively, indicating all the blend films should have good interface contact with the electrode. The BT-ER-based film shows a continuous interpenetrating network with proper phase separation and smoother morphology than BT-CN-based film, which is benefitting to exciton dissociation and charge transport in the ternary device. As shown in Figure S15, Supporting Information, the BT-CN:Y6 and BT-ER:Y6 blend film present larger domain size with RMS value of 3.95 nm for BT-CN:Y6 and 2.41 nm for BT-ER:Y6, which is obstructed to the exciton dissociation and charge transport, thereby resulting in low PCE value in the binary device.

To further investigate the orientation and packing behaviors, grazing-incidence wide-angle X-ray scattering (GIWAXS) measurement was conducted. The 2D GIWAXS patterns and 1D line cuts of the blend films are shown in Figure 4g-j and the packing parameters are summarized in **Table 3**. As shown

Table 3. GIWAXS data of the PM6:Y6, PM6:BT-CN:Y6, and PM6:BT-ER:Y6 blend films.

Film	(010) diffraction peak				(100) diffraction peak			
	Q [Å^{-1}]	D [Å]	FWHM [Å^{-1}]	CCL [Å]	Q [Å^{-1}]	D [Å]	FWHM [Å^{-1}]	CCL [Å]
PM6:Y6	1.75	3.59	0.262	23.97	0.29	21.66	0.154	40.78
PM6:BT-CN:Y6	1.72	3.65	0.244	25.74	0.29	21.66	0.096	65.42
PM6:BT-ER:Y6	1.71	3.67	0.225	27.91	0.28	22.43	0.09	69.78

Obtained using the equation of D = 2π/Q, in which Q is the corresponding x-coordinate of the diffraction peak. CCL is Calculated using the equation: CCL = 2πK/w, in which w is the full-width-at-half maximum (FWHM) and K is a form factor (0.9 here).

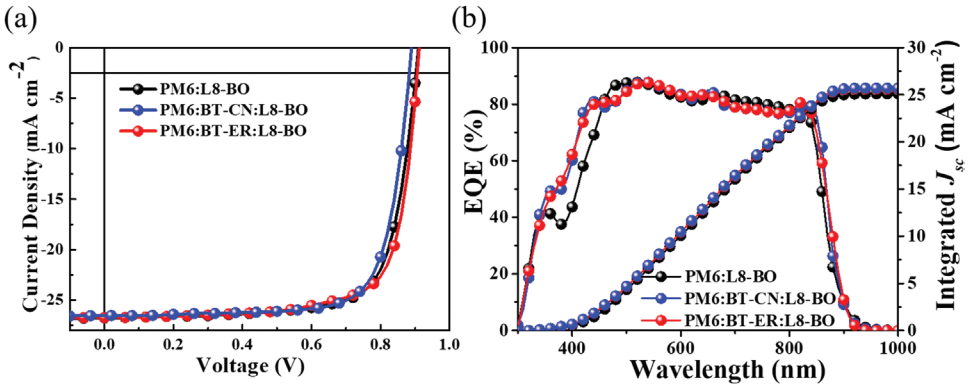

Figure 5. Photovoltaic performance of the L8-BO-based binary and ternary optimized OSCs a) *J–V* curves. b) EQE curves.

in Figure S16, Supporting Information, the neat BT-CN film displays a diffraction peak in the out-of-plane (OOP) and (010) diffraction peak in the in-plane (IP) direction, implying a high degree of molecular ordering. Whereas the neat BT-ER film exhibits a weak scattering feature, indicating relatively low crystallinity. As we can see from Figure 4g–j, the PM6:Y6 blend film shows a (010) peak at 1.75 $Å^{-1}$ (d = 3.59 Å) in the OOP direction and a strong diffraction (100) peak at 0.29 $Å^{-1}$ (d = 21.66 Å) in the IP direction, suggesting the preferential face-on orientation. The BT-CN-based ternary film shows a (010) peak at 1.72 $Å^{-1}$ (d = 3.65 Å) in the OOP direction with a crystal coherence length (CCL) of 25.74 Å. BT-ER-based ternary film exhibits a stronger (010) peak at 1.71 $Å^{-1}$ (d = 3.67 Å) in OOP direction with CCL value of 27.91 Å and a diffraction (100) peak at 0.28 $Å^{-1}$ (d = 22.43 Å) in the IP direction (Table 3). Compared with the PM6:Y6 binary film, the enhanced CCL value of the ternary film demonstrates a higher crystallinity and more orderly orientation, which is beneficial to charge dissociation and transport, and consistent with the enhanced J_{SC} and FF in the ternary device. Besides, the ternary blend based on BT-ER shows slightly higher crystallinity than that of BT-CN-based ternary blend, which partially contributes to its slightly higher PCE of BT-ER-based ternary device.

2.5. Additional Device

To study the universality of these two SM donors as the third component, ternary OSCs with device architecture of ITO/PEDOT:PSS/PM6:BT-CN(BT-ER):L8-BO/PNDIT-F3N/Ag have also been fabricated and the detailed optimization data is shown in Tables S8–S11, Supporting Information. The device based on PM6:L8-BO exhibits a PCE of 17.55% with V_{OC} of 0.888 V, J_{SC} of 26.14 mA cm^{-2} and FF of 75.6%. As shown in Table 1 and **Figure 5**, when introducing BT-CN or BT-ER into PM6:L8-BO host, the PCE has been enhanced from 17.55% to 18.05% and 18.11% for BT-CN or BT-ER, respectively, mainly contributing from the increased V_{OC} and J_{SC}. Hence, the ascending PCE can primarily be ascribed to the good miscibility with PM6 and complementary absorption of the two SM donors.

3. Conclusion

In summary, two SM donors, BT-CN and BT-ER with different end-groups were designed and synthesized as the second donor component for high efficient ternary device. Both molecules exhibit complementary absorption with PM6:Y6 system. As confirmed by differential scanning calorimetry and surface free energy, both SM donors are confirmed to show good compatibility with PM6 than Y6, contributing to the nanofibrous phases in the ternary device. Higher charge mobilities were obtained in the optimal ternary device as a result of the enhanced face-on molecular packing, which promotes charge collection and reduces carrier recombination. Therefore, ternary OSCs with 20 wt.% BT-CN and BT-ER achieved a PCE of 16.8% and 17.22% due to the synchronously increased V_{OC}, $J_{SC,}$ and FF compared with the PM6:Y6 binary device. Furthermore, both SMs were further used as guest donors of the PM6:L8-BO system, which leads to an increased V_{OC} and J_{SC} as well, hence, an impressive efficiency of 18.05% and 18.11% were achieved when incorporating BT-CN and BT-ER, respectively, demonstrating the applicability of these two SM donors compatibility with other PM6 based binary devices. Overall, this work shows that BDTT-SiCl-substituted molecules are a promising class of SM donors for high-performance ternary OSCs.

Supporting Information

Supporting Information is available from the Wiley Online Library or from the author.

Acknowledgements

J.L. and C.Z. contributed equally to this work. The authors thank the financial support from the NSF of China (62104197; 62004129). H.H thanks the financial support from the Scientific Research Startup Fund for Shenzhen High-Caliber Personnel of Shenzhen Polytechnic, No. 6022310038k, and 6022310049k.

Conflict of Interest

The authors declare no conflict of interest.

Data Availability Statement

The data that support the findings of this study are available from the corresponding author upon reasonable request.

Keywords

effect of end group, small molecular donors, ternary organic solar cells

Received: September 8, 2022
Revised: October 30, 2022
Published online: November 18, 2022

[1] C. Yan, S. Barlow, Z. Wang, H. Yan, A. Jen, S. Marder, X. Zhan, *Nat. Rev. Mater.* **2018**, *3*, 18003.
[2] J. Wang, H. Yao, Y. Xu, L. Ma, J. Hou, *Mater. Chem. Front.* **2021**, *5*, 709.
[3] S. Park, T. Kim, S. Yoon, C. Koh, H. Woo, H. Son, *Adv. Mater.* **2020**, *32*, 2002217.
[4] L. Lu, T. Zheng, Q. Wu, A. Schneider, D. Zhao, L. Yu, *Chem. Rev.* **2015**, *115*, 12666.
[5] G. Wang, M. Adil, J. Zhang, Z. Wei, *Adv. Mater.* **2019**, *31*, 1805089.
[6] K. Jiang, Q. Wei, J. Lai, Z. Peng, H. Kim, J. Yuan, L. Ye, H. Ade, Y. Zou, H. Yan, *Joule* **2019**, *3*, 3020.
[7] J. Yuan, T. Huang, P. Cheng, Y. Zou, H. Zhang, J. Yang, S. Chang, Z. Zhang, W. Huang, R. Wang, D. Meng, F. Gao, Y. Yang, *Nat. Commun.* **2019**, *10*, 570.
[8] Y. Cui, H. Yao, J. Zhang, T. Zhang, Y. Wang, L. Hong, K. Xian, B. Xu, S. Zhang, J. Peng, Z. Wei, F. Gao, J. Hou, *Nat. Commun.* **2019**, *10*, 2515.
[9] S. Liu, J. Yuan, W. Deng, M. Luo, Y. Xie, Q. Liang, Y. Zou, Z. He, H. Wu, Y. Cao, *Nat. Photonics* **2020**, *14*, 300.
[10] R. Wang, J. Yuan, R. Wang, G. Han, T. Huang, W. Huang, J. Xue, H. Wang, C. Zhang, C. Zhu, P. Cheng, D. Meng, Y. Yi, K. Wei, Y. Zou, Y. Yang, *Adv. Mater.* **2019**, *31*, 1904215.
[11] Y. Cui, H. Yao, J. Zhang, K. Xian, T. Zhang, L. Hong, Y. Wang, Y. Xu, K. Ma, C. An, C. He, Z. Wei, F. Gao, J. Hou, *Adv. Mater.* **2020**, *32*, 1908205.
[12] X. Kong, C. Zhu, J. Zhang, L. Meng, S. Qin, J. Zhang, J. Li, Z. Wei, Y. Li, *Energy Environ. Sci.* **2022**, *15*, 2011.
[13] M. Wang, J. Lin, Z. Zheng, L. Zhu, P. Bi, H. Liang, X. Guo, J. Wu, Y. Wang, L. Yu, J. Li, J. Lv, X. Liu, F. Liu, Y. Li, *Energy Environ. Sci.* **2022**, *15*, 1585.
[14] Y. Cui, Y. Xu, H. Yao, P. Bi, L. Hong, J. Zhang, Y. Zu, T. Zhang, J. Qin, J. Ren, Z. Chen, C. He, X. Hao, Z. Wei, J. Hou, *Adv. Mater.* **2021**, *33*, 2102420.
[15] Y. Jin, Y. Zhang, Y. Liu, J. Xue, W. Li, J. Qiao, F. Zhang, *Adv. Mater.* **2019**, *31*, 1900690.
[16] L. Zhu, M. Zhang, W. Zhong, S. Leng, G. Zhou, Y. Zou, X. Su, H. Ding, P. Gu, F. Liu, Y. Zhang, *Energy Environ. Sci.* **2021**, *14*, 4341.
[17] J. Yuan, Y. Zhang, L. Zhou, G. Zhang, H. Yip, T. Lau, X. Lu, C. Zhu, H. Peng, P. Johnson, M. Leclerc, Y. Cao, J. Ulanski, Y. Li, Y. Zou, *Joule* **2019**, *3*, 1140.
[18] H. Yang, Y. Dong, H. Fan, Y. Wu, C. Cui, Y. Li, *Sol. RRL* **2021**, *5*, 2100013.
[19] Y. Yan, Y. Zhang, Y. Liu, Y. Shi, D. Qiu, D. Deng, J. Zhang, B. Wang, M. Adil, K. Amin, W. Memon, M. Wang, H. Zhou, X. Zhang, Z. Wei, *Adv. Energy Mater.* **2022**, *12*, 2200129.
[20] S. Bao, H. Yang, J. Zhang, Z. Wei, C. Cui, Y. Li, *Adv. Mater.* **2021**, *33*, 2105301.
[21] H. Chen, H. Lai, Z. Chen, Y. Zhu, H. Wang, L. Han, Y. Zhang, F. He, *Angew. Chem., Int. Ed.* **2021**, *60*, 3238.
[22] Y. Zhang, B. Kan, Y. Sun, Y. Wang, R. Xia, X. Ke, Y. Q. Yi, C. Li, H. L. Yip, X. Wan, Y. Cao, Y. Chen, *Adv. Mater.* **2018**, *30*, 1707508.
[23] M. Xiao, K. Zhang, S. Dong, Q. Yin, Z. Liu, L. Liu, F. Huang, Y. Cao, *ACS Appl. Mater. Interfaces* **2018**, *10*, 25594.
[24] X. Ma, Y. Mi, F. Zhang, Q. An, M. Zhang, Z. Hu, X. Liu, J. Zhang, W. Tang, *Adv. Energy Mater.* **2018**, *8*, 1702854.
[25] D. Zhou, W. You, H. Xu, Y. Tong, B. Hu, Y. Xie, L. Chen, *J. Mater. Chem. A* **2020**, *8*, 23096.
[26] C. Zhao, J. Wang, X. Zhao, Z. Du, R. Yang, J. Tang, *Nanoscale* **2021**, *13*, 2181.
[27] T. Yan, J. Ge, T. Lei, W. Zhang, W. Song, B. Fanady, D. Zhang, S. Chen, R. Peng, Z. Ge, *J. Mater. Chem. A* **2019**, *7*, 25894.
[28] X. Chen, Q. Zhang, D. Wang, X. Xu, Z. Wang, Y. Li, H. Zhu, X. Lu, W. Chen, H. Qiu, C. Li, *Sol. RRL* **2020**, *4*, 2000537.
[29] Y. Q. C. An, T. Zhang, Q. Lv, J. Qin, S. Zhang, C. He, *J. Mater. Chem. A* **2021**, *9*, 13653.
[30] T. Zhang, N. Gasparini, *Appl. Phys. Lett.* **2022**, *120*, 250501.
[31] L. Zhan, S. Li, Y. Li, R. Sun, J. Min, Y. Chen, J. Fang, C. Ma, G. Zhou, H. Zhu, L. Zuo, H. Qiu, S. Yin, H. Chen, *Adv. Energy Mater.* **2022**, *12*, 2201076.
[32] X. Duan, W. Song, J. Qiao, X. Li, Y. Cai, H. Wu, J. Zhang, X. Hao, Z. Tang, Z. Ge, F. Huang, Y. Sun, *Energy Environ. Sci.* **2022**, *15*, 1563.
[33] M. Zhang, L. Zhu, T. Hao, G. Zhou, C. Qiu, Z. Zhao, N. Hartmann, B. Xiao, Y. Zou, W. Feng, H. Zhu, M. Zhang, Y. Zhang, Y. Li, T. Russell, F. Liu, *Adv. Mater.* **2021**, *33*, 2007177.
[34] Q. Lv, C. An, T. Zhang, J. Zhang, S. Zhang, P. Zhou, C. He, J. Hou, *Chem* **2021**, *64*, 1200.
[35] H. Tang, T. Xu, C. Yan, J. Gao, H. Yin, J. Lv, R. Singh, M. Kumar, T. Duan, Z. Kan, S. Lu, G. Li, *Adv. Sci.* **2019**, *6*, 1901613.
[36] J. Wang, Q. Yin, J. Miao, Z. Wu, Z. Chang, Y. Cao, R. Zhang, J. Wang, H. Wu, Y. Cao, *Adv. Funct. Mater.* **2015**, *25*, 3514.
[37] K. Sun, Z. Xiao, S. Lu, W. Zajaczkowski, W. Pisula, E. Hanssen, J. White, R. Williamson, J. Subbiah, J. Ouyang, A. Holmes, W. Wong, D. Jones, *Nat. Commun.* **2015**, *6*, 6013.
[38] J. Zhou, X. Wan, Y. Liu, Y. Zuo, Z. Li, G. He, G. Long, W. Ni, C. Li, X. Su, Y. Chen, *J. Am. Chem. Soc.* **2012**, *134*, 16345.
[39] H. Wang, F. Du, J. Cao, J. Yu, X. Liu, W. Tang, *Chem. Eng. J.* **2022**, *428*, 132640.
[40] X. Ding, X. Chen, Y. Xu, Z. Ni, T. He, H. Qiu, C. Li, Q. Zhang, *Chem. Eng. J.* **2022**, *429*, 132298.
[41] C. Zhang, Y. Zhang, L. Wang, H. Wu, B. Wu, Z. Tang, W. Ma, Z. Luo, C. Li, Z. Bo, C. Yang, *Chem. Eng. J.* **2022**, *446*, 137206.
[42] W. Feng, S. Wu, H. Chen, L. Meng, F. Huang, H. Liang, J. Zhang, Z. Wei, X. Wan, C. Li, Z. Yao, Y. Chen, *Adv. Energy Mater.* **2022**, *12*, 2104060.
[43] B. Li, Q. Zhang, S. Li, X. Yang, F. Yang, Y. Kong, Y. Li, Z. Wu, W. Zhang, Q. Zhao, Y. Zhang, H. Y. Woo, J. Yuan, W. Ma, *Chem. Eng. J.* **2022**, *438*, 135543.
[44] L. Xu, W. Tao, H. Liu, J. Ning, M. Huang, B. Zhao, X. Lu, S. Tan, *J. Mater. Chem. A* **2021**, *9*, 11734.
[45] M. Guan, W. Tao, L. Xu, Y. Qin, J. Zhang, S. Tan, M. Huang, B. Zhao, *J. Mater. Chem. A* **2022**, *10*, 9746.
[46] Z. Chen, W. Song, K. Yu, J. Ge, J. Zhang, L. Xie, R. Peng, Z. Ge, *Joule* **2021**, *5*, 2395.
[47] B. Qiu, Z. Chen, S. Qin, J. Yao, W. Huang, L. Meng, H. Zhu, Y. Yang, Z. Zhang, Y. Li, *Adv. Mater.* **2020**, *32*, 1908373.
[48] J. Zhou, Y. Zuo, X. Wan, G. Long, Q. Zhang, W. Ni, Y. Liu, Z. Li, G. He, C. Li, B. Kan, M. Li, Y. Chen, *J. Am. Chem. Soc.* **2013**, *135*, 8484.
[49] R. Zhou, Z. Jiang, Y. Shi, Q. Wu, C. Yang, J. Zhang, K. Lu, Z. Wei, *Adv. Funct. Mater.* **2020**, *30*, 2005426.
[50] Z. Ji, X. Xu, G. Zhang, Y. Li, Q. Peng, *Nano Energy* **2017**, *40*, 214.
[51] X. Dong, K. Yang, H. Tang, D. Hu, S. Chen, J. Zhang, Z. Kan, T. Duan, C. Hu, X. Dai, Z. Xiao, K. Sun, S. Lu, *Sol. RRL* **2019**, *4*, 1900326.

[52] H. Bin, Y. Yang, Z. Zhang, L. Ye, M. Ghasemi, S. Chen, Y. Zhang, C. Zhang, C. Sun, L. Xue, C. Yang, H. Ade, Y. Li, *J. Am. Chem. Soc.* **2017**, *139*, 5085.
[53] H. Bin, I. Angunawela, B. Qiu, F. Colberts, M. Li, M. Dyson, M. Wienk, H. Ade, Y. Li, R. Janssen, *Adv. Energy Mater.* **2020**, *10*, 2001589.
[54] X. Chen, D. Wang, Z. Wang, Y. Li, H. Zhu, X. Lu, W. Chen, H. Qiu, Q. Zhang, *Chem. Eng. J.* **2021**, *424*, 130397.
[55] T. Duan, H. Tang, R. Liang, J. Lv, Z. Kan, R. Singh, M. Kumar, Z. Xiao, S. Lu, F. Laquai, *J. Mater. Chem. A* **2019**, *7*, 2541.
[56] W. Su, Y. Wang, Z. Yin, Q. Fan, X. Guo, L. Yu, Y. Li, L. Hou, M. Zhang, Q. Peng, Y. Li, E. Wang, *ChemSusChem* **2021**, *14*, 3535.
[57] W. Su, G. Li, Q. Fan, Q. Zhu, X. Guo, J. Chen, J. Wu, W. Ma, M. Zhang, Y. Li, *J. Mater. Chem. A* **2019**, *7*, 2351.
[58] H. Bin, J. Yao, Y. Yang, I. Angunawela, C. Sun, L. Gao, L. Ye, B. Qiu, L. Xue, C. Zhu, C. Yang, Z. Zhang, H. Ade, Y. Li, *Adv. Mater.* **2018**, *30*, 1706361.
[59] G. Xie, Z. Zhang, Z. Su, X. Zhang, J. Zhang, *Nano Energy* **2020**, *69*, 104447.
[60] Y. Ma, D. Cai, S. Wan, P. Wang, J. Wang, Q. Zheng, *Angew. Chem., Int. Ed.* **2020**, *59*, 21627.
[61] J. Bredas, *Mater. Horiz.* **2014**, *1*, 17.
[62] Q. Wei, S. Liang, W. Liu, Y. Hu, B. Qiu, J. Ren, J. Yuan, F. Huang, Y. Zou, Y. Li, *ACS Energy Lett.* **2022**, *7*, 2373.
[63] K. Vandewal, K. Tvingstedt, A. Gadisa, O. Inganas, J. Manca, *Nat. Mater.* **2009**, *8*, 904.
[64] G. Chai, J. Zhang, M. Pan, Z. Wang, J. Yu, J. Liang, H. Yu, Y. Chen, A. Shang, X. Liu, F. Bai, R. Ma, Y. Chang, S. Luo, A. Zeng, H. Zhou, K. Chen, F. Gao, H. Ade, H. Yan, *ACS Energy Lett.* **2020**, *5*, 3415.
[65] D. Cai, J. Zhang, J. Wang, Y. Ma, S. Wan, P. Wang, Z. Wei, Q. Zheng, *J. Mater. Chem. A* **2020**, *8*, 24543.
[66] M. Jeong, J. Oh, Y. Cho, B. Lee, S. Jeong, S. M. Lee, S. H. Kang, C. Yang, *Adv. Funct. Mater.* **2021**, *31*, 2102371.
[67] S. Jung, Y. Cho, S.-H. Kang, S.-J. Yoon, C. Yang, *Sol. RRL* **2021**, *6*, 2100819.
[68] Z. Luo, T. Liu, Y. Wang, G. Zhang, R. Sun, Z. Chen, C. Zhong, J. Wu, Y. Chen, M. Zhang, Y. Zou, W. Ma, H. Yan, J. Min, Y. Li, C. Yang, *Adv. Energy Mater.* **2019**, *9*, 1900041.
[69] X.-K. Chen, D. Qian, Y. Wang, T. Kirchartz, W. Tress, H. Yao, J. Yuan, M. Hülsbeck, M. Zhang, Y. Zou, Y. Sun, Y. Li, J. Hou, O. Inganäs, V. Coropceanu, J. Bredas, F. Gao, *Nat. Energy* **2021**, *6*, 799.
[70] X. Jiang, J. Yang, S. Karuthedath, J. Li, W. Lai, C. Li, C. Xiao, L. Ye, Z. Ma, Z. Tang, F. Laquai, W. Li, *Angew. Chem., Int. Ed.* **2020**, *59*, 21683.
[71] T. Chen, J. Yu, Y. Lin, S. Peng, S. Wu, Y. Su, V. Karapala, L. Hong, H. Yao, J. Hou, C. Hsu, *Sol. RRL* **2020**, *4*, 2000357.